

Electronic Supplementary Information

Anisotropy-Dependent Chirality Transfer from Cellulose Nanocrystals to β -FeOOH Nanowhiskers

Jinyu Tang,¹ Shouhua Feng,¹ and Ming Yang^{1,}*

¹ The State Key Laboratory of Inorganic Synthesis and Preparative Chemistry, Jilin University, 2699
Qianjin Street, Changchun, 130012, Jilin

*Corresponding Author(s): mingyang@jlu.edu.cn

Section S1. Supplementary Data

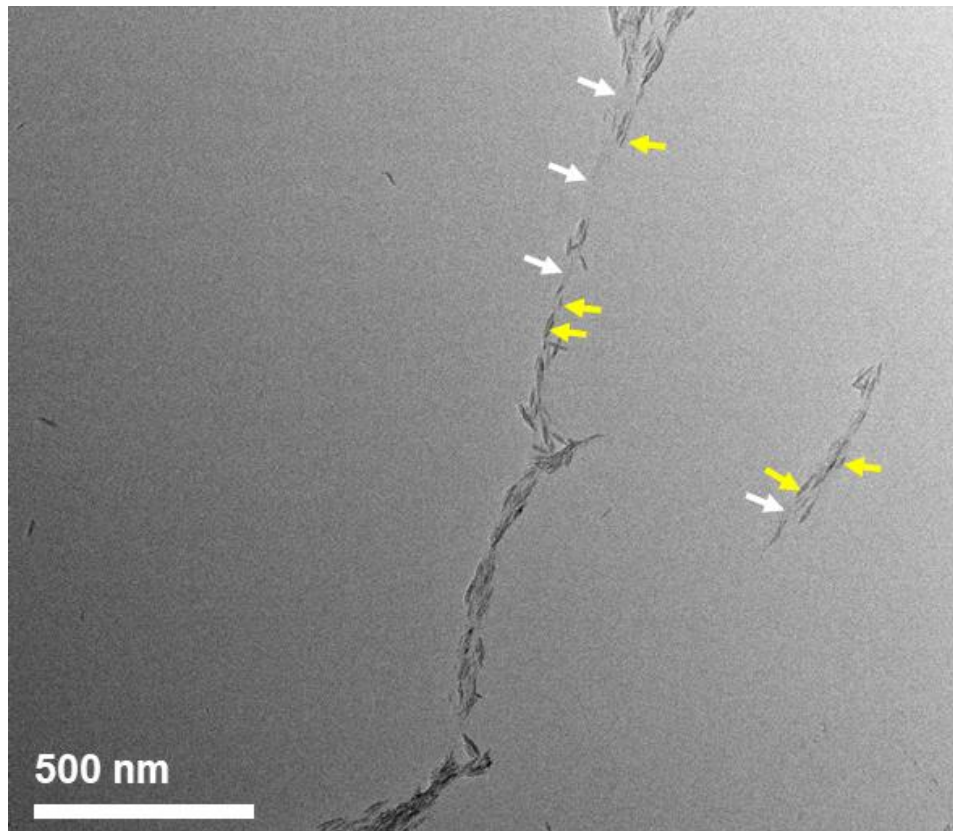


Figure S1. A low-magnification TEM image of CNC-Fe-36. The white and yellow arrows indicate the presence of CNCs and NWs, respectively.

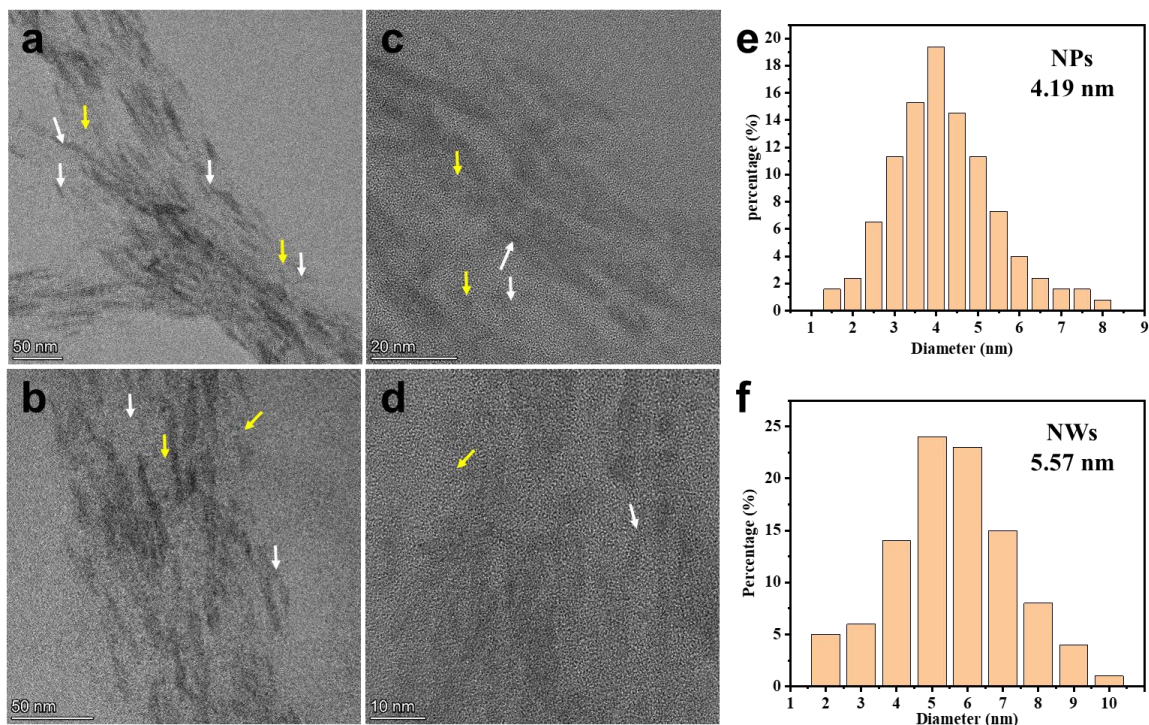


Figure S2. (a-d) TEM images of CNC-Fe-36 with different magnifications. The white and yellow arrows indicate the presence of NWs and NPs, respectively. (e, f) Histogram of diameter distributions of NPs and NWs.

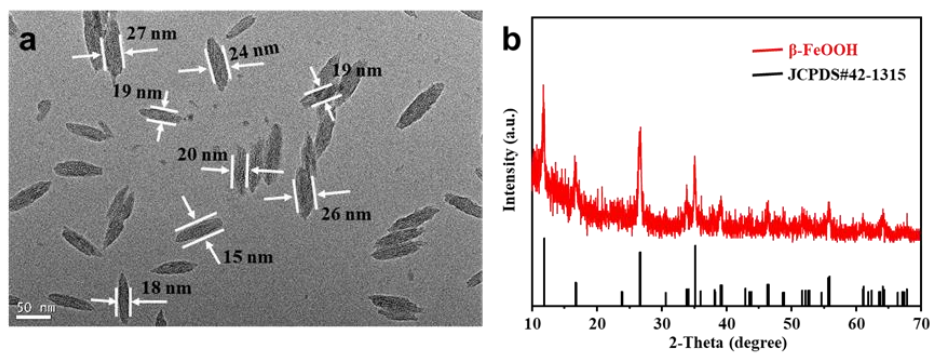


Figure S3. (a) A TEM image and (b) the XRD pattern of β -FeOOH obtained in the absence of CNCs.

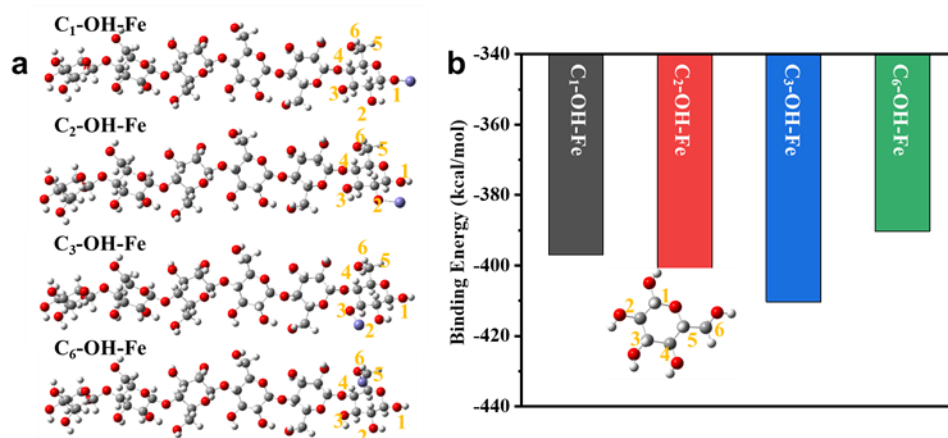


Figure S4. (a) Molecular models used for the calculation of binding energies at different sites. (b) The calculated results showing the preferred interaction between C₃-OH and Fe.

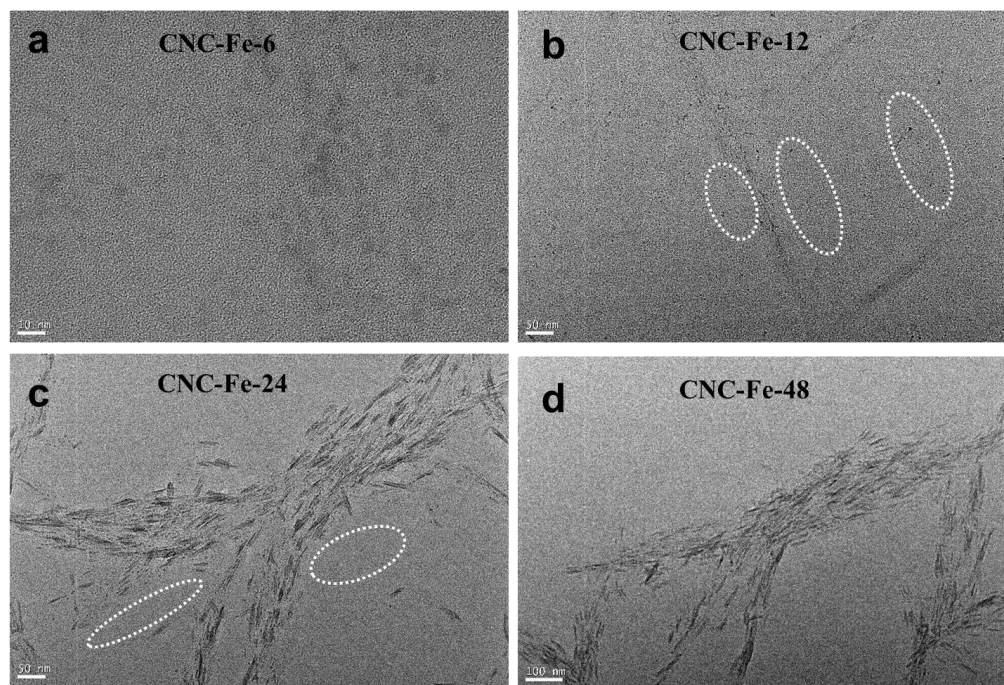


Figure S5. TEM images of (a) CNC-Fe-6, (b) CNC-Fe-12, (c) CNC-Fe-24 and (d) CNC-Fe-48. The circles in b and c show the free NPs that are not associated with CNCs.

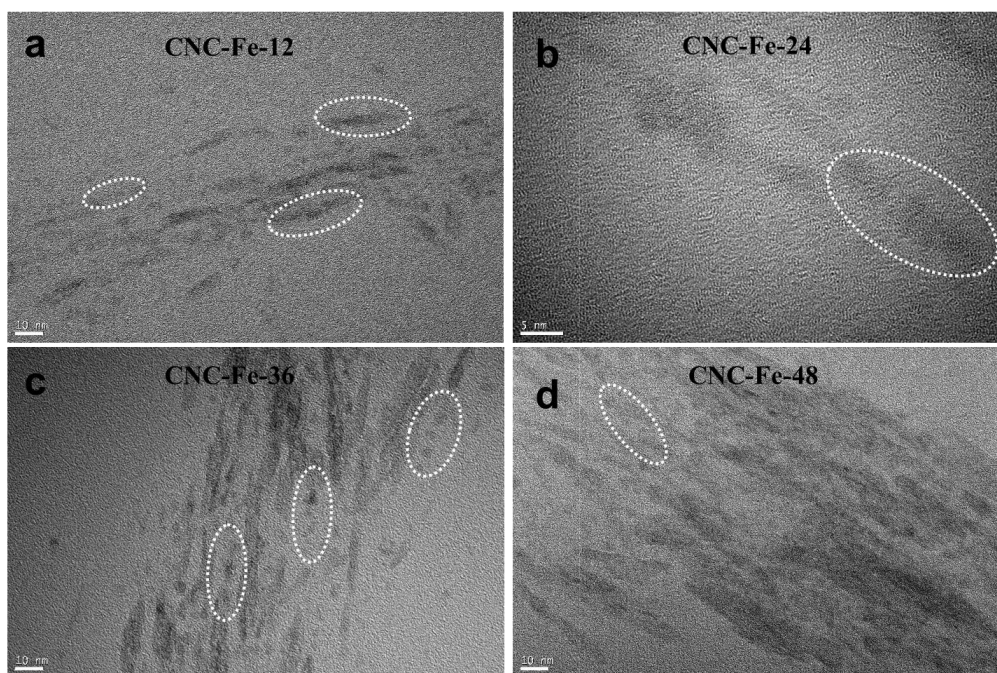


Figure S6. TEM images showing the linear arrangement of NPs on the surface of CNCs.

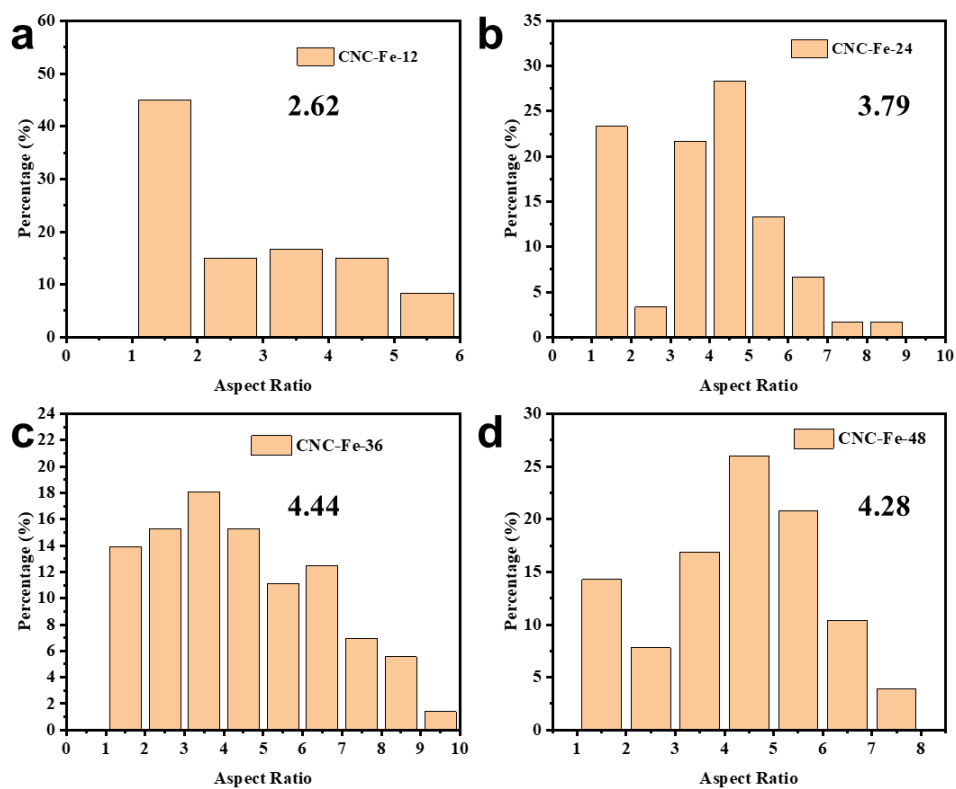


Figure S7. ARs of β -FeOOH from CNC-Fe-12, CNC-Fe-24, CNC-Fe-36 and CNC-Fe-48.

Table S1. Zeta potential of CNCs before and after the addition of Fe^{3+} . The concentration is 0.1 wt%.

Sample	CNC	CNC- Fe^{3+}
Zeta potential (mV)	-65.8	-8.2

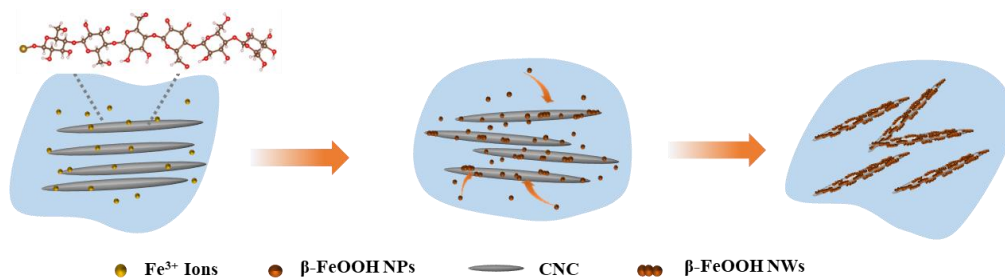


Figure S8. Schematic illustration of orientation attachment of $\beta\text{-FeOOH}$ on the surface of CNCs.

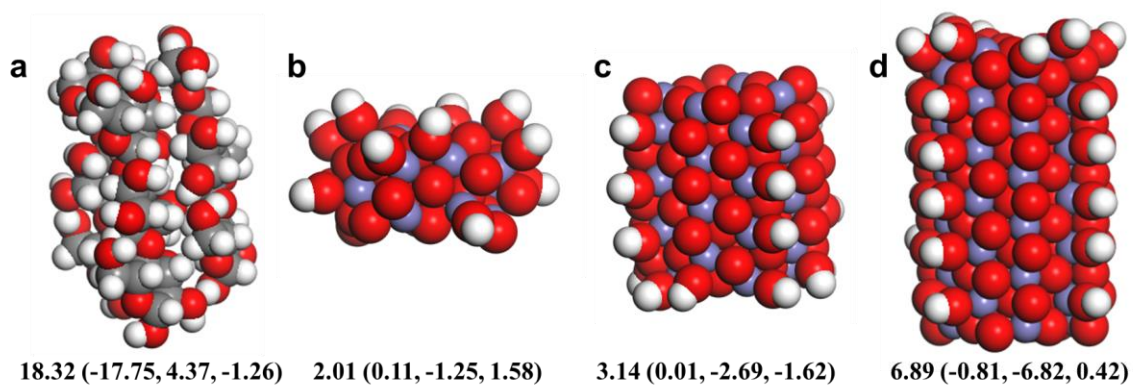


Figure S9. Ball-and-stick models and corresponding calculation results of DMs for (a) a three antiparallel chain model each containing three $\beta\text{-1,4}$ -linked D-glucose units and (b-d) iron oxide clusters with different aspect ratios: (b) 1, (c) 2, and (d) 3.

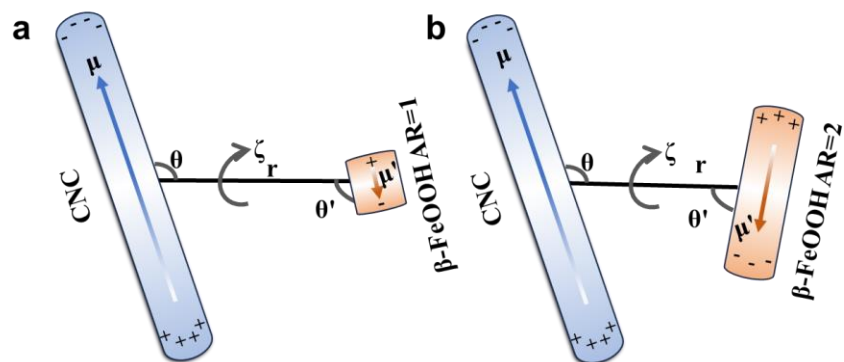


Figure S10. The schematic for the calculation of dipole-dipole interaction energies between CNCs and β -FeOOH with (a) AR=1 and (b) AR=2.

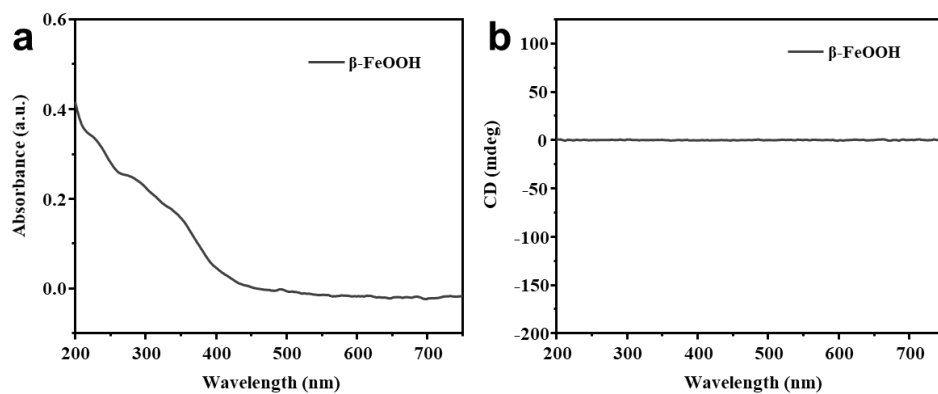


Figure S11. (a) UV-vis and (b) CD spectra of β -FeOOH dispersions obtained in the absence of CNCs.

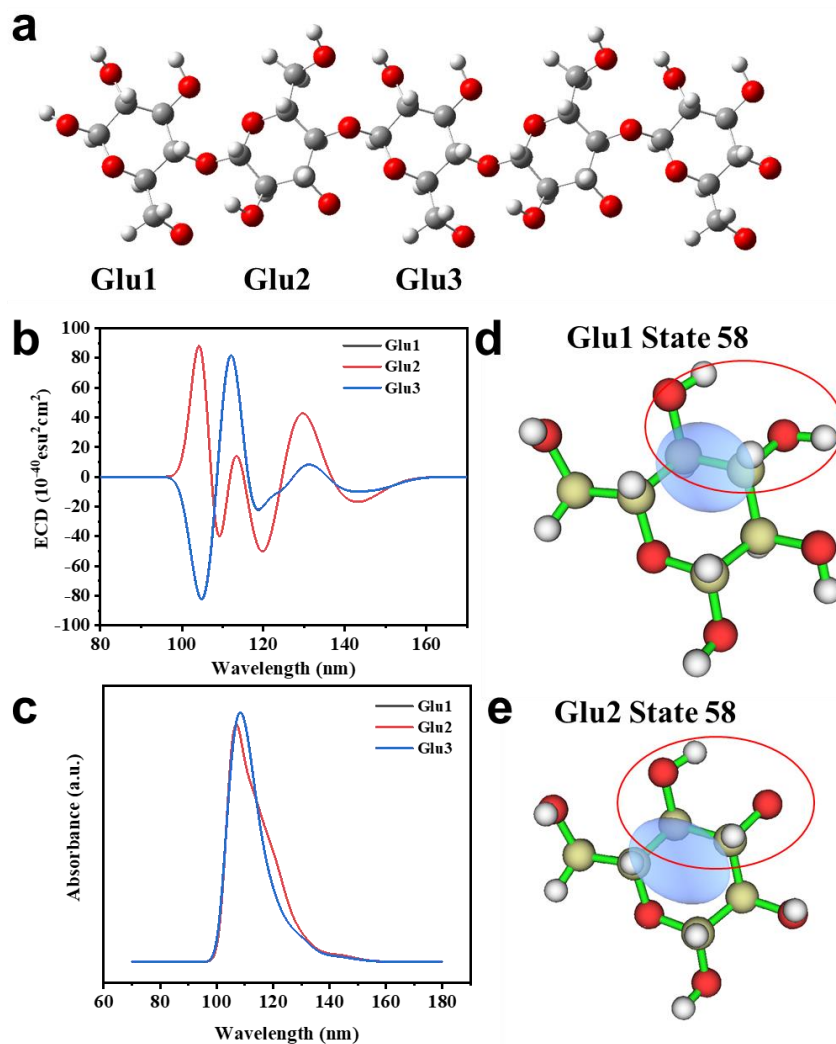


Figure S12. TD-DFT calculation results of a D-glucopyranose unit extracted from the structure of CNCs at different positions. (a) A cellulose chain containing five glucose monomers linked by β -(1-4) glycosidic bonds. Glu1-3 represents the first, second, and third D-glucopyranose unit from the left. Simulated (b) CD and (c) absorbance spectra of Glu1-3. (d) and (e) are the differential charge density of the 58th excited state for Glu1 and Glu2, respectively. The peak at 104 nm shows a reverse signal for Glu1 and Glu2, which can be attributed to the different orientations of -OH groups. Glu1 (the black line in b and c) and Glu3 (the blue line in b and c) display identical signals because of the same structure.

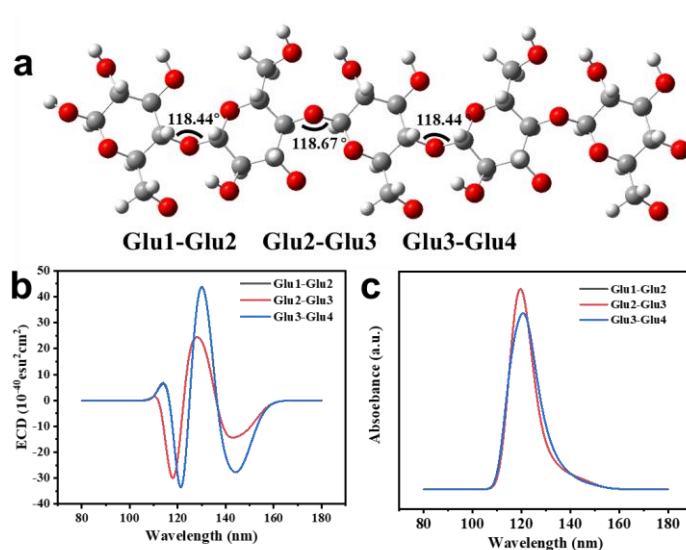


Figure S13. TD-DFT calculation results of two glucose monomers linked by β -(1–4) glycosidic bonds (Glu) extracted from the structure of cellulose at different positions. (a) A cellulose chain containing five glucose monomers linked by β -(1–4) glycosidic bonds. Glu1-Glu2, Glu2-Glu3 and Glu3-Glu4 represent two glucose monomers extracted from different positions counting from the left. Simulated (b) CD and (c) absorbance spectra of Glu1-Glu2, Glu2-Glu3 and Glu3-Glu4. Glu1-Glu2 (the black line in b and c) and Glu3-Glu4 (the blue line in b and c) display identical signals because of the same structure.

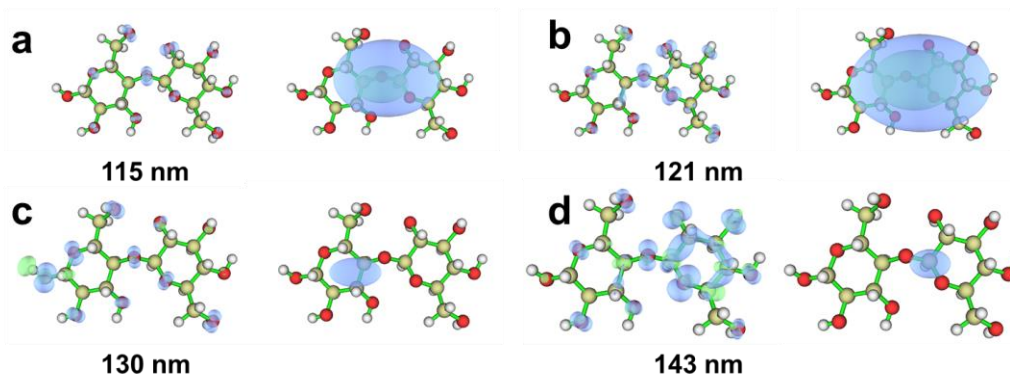


Figure S14. Hole-electron distribution (left) and charge differential density (right) plot for Glu at (a) 115 nm (Excited State 58), (b) 121 nm (Excited State 36), (c) 130 nm (Excited State 17) and (d) 143 nm (Excited State 6). The green color in the figure represents the electron distribution, while the blue color represents the hole distribution. This figure reflected the process of major electron transitions. The change of hole-electron distribution corresponds to the main transition of Glu. σ to σ^* and n to σ^* transition made great contributions to the spectra.

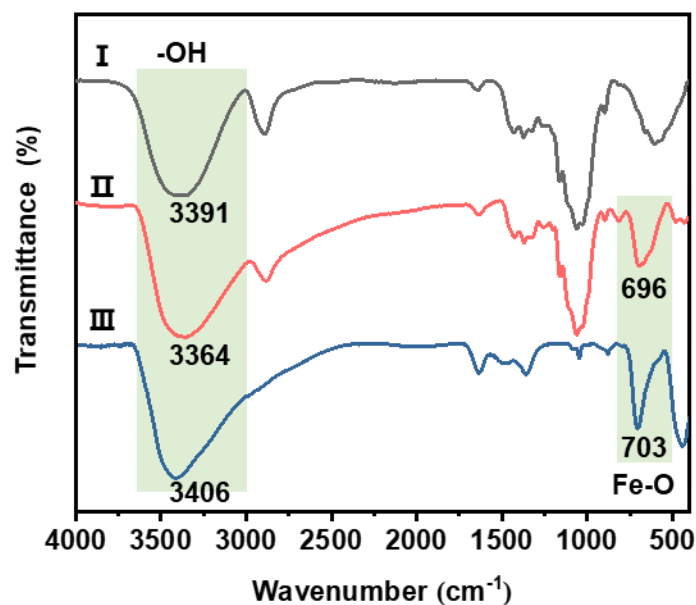


Figure S15. FT-IR spectra of (I) CNCs, (II) CNC-Fe-36 and (III) β -FeOOH.

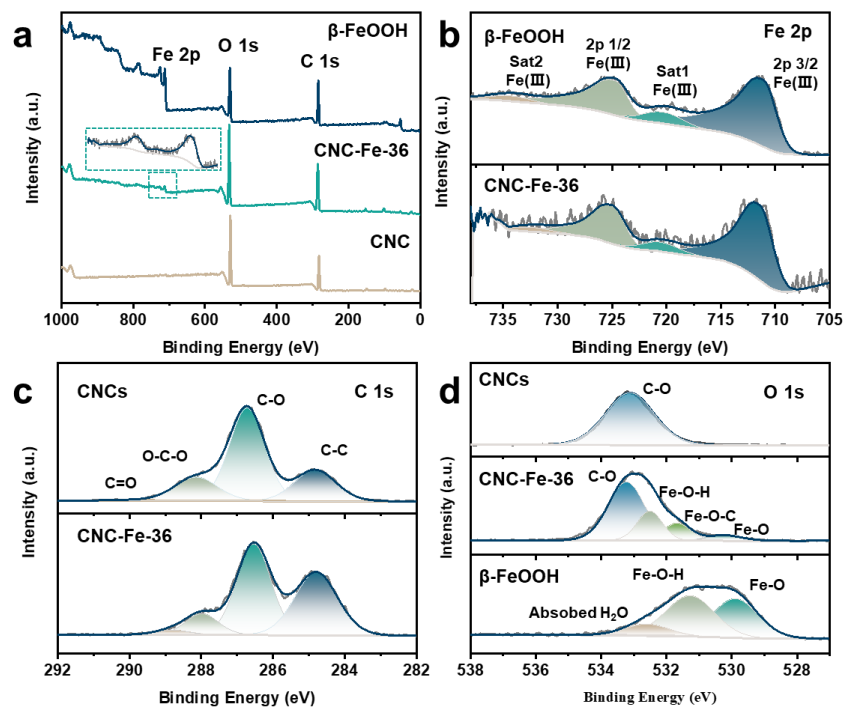


Figure S16. XPS spectra of β -FeOOH, CNC-Fe-36, and CNCs. (a) Full range scan, (b) Fe 2p, (c) C 1s and (d) O 1s.

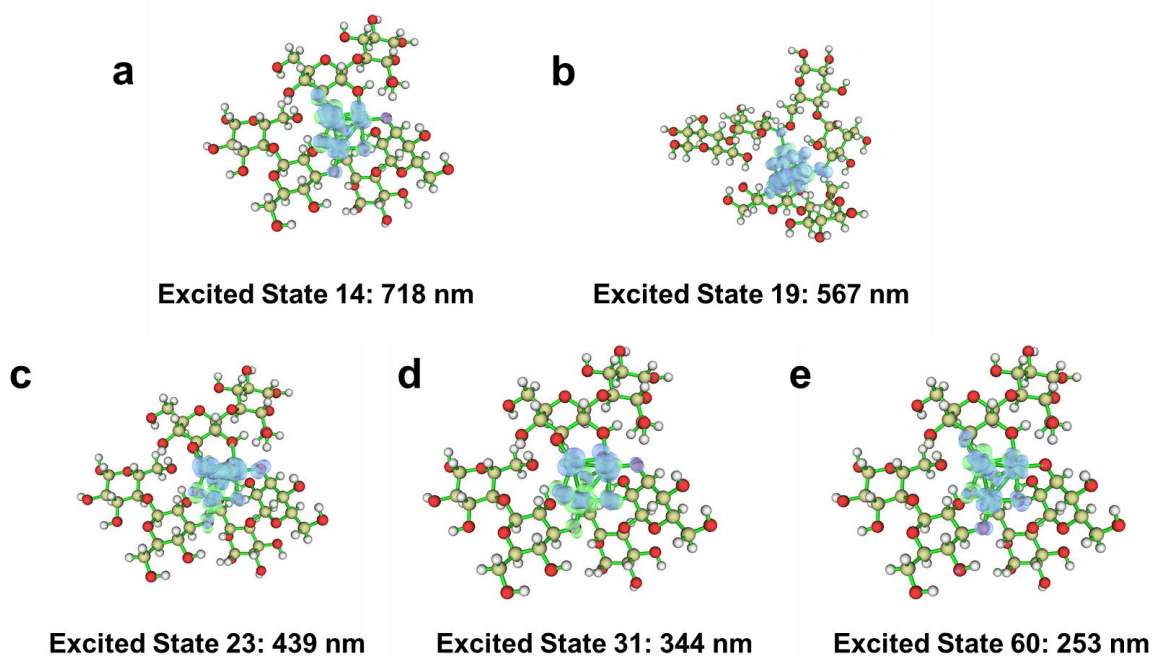


Figure S17. Hole-electron distribution of $\text{Fe}_3\text{O}_6\text{-3Glu}$ in Multiwfn. (a) Excited State 14, (b) Excited State 19, (c) Excited State 23, (d) Excited State 31, and (e) Excited State 60.

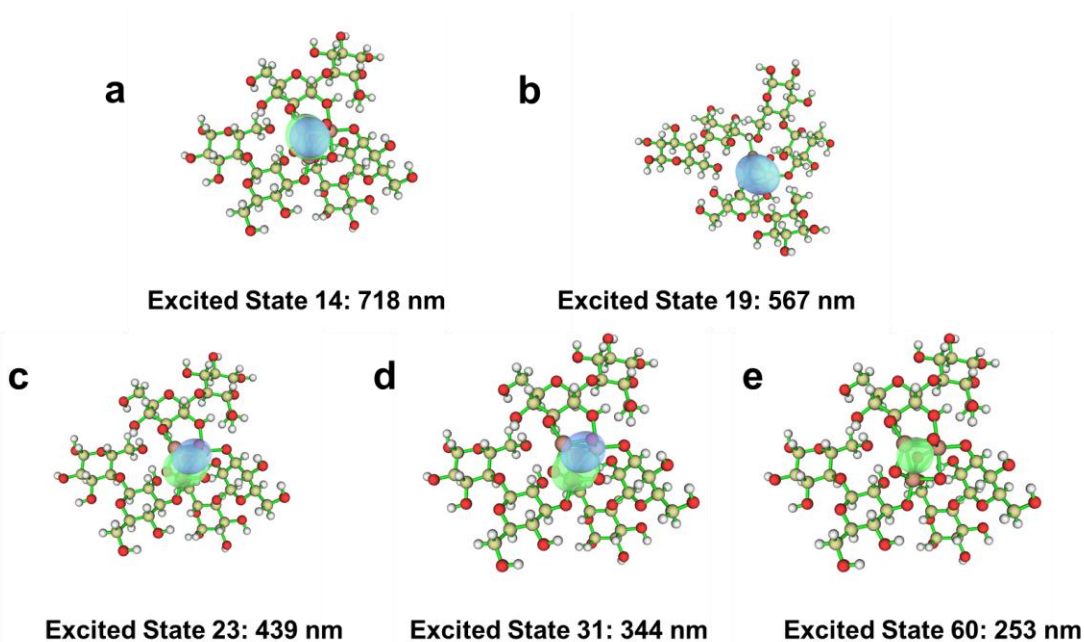


Figure S18. $C_{\text{Hole}}\text{-}C_{\text{electron}}$ distribution of $\text{Fe}_3\text{O}_6\text{-3Glu}$ in Multiwfn. (a) Excited State 14, (b) Excited State 19, (c) Excited State 23, (d) Excited State 31, and (e) Excited State 60.

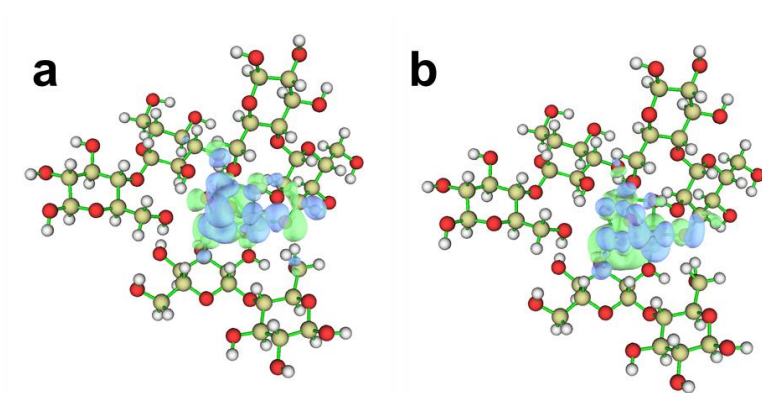


Figure S19. (a) HOMO and (b) LUMO for $\text{Fe}_3\text{O}_6\text{-3Glu}$.

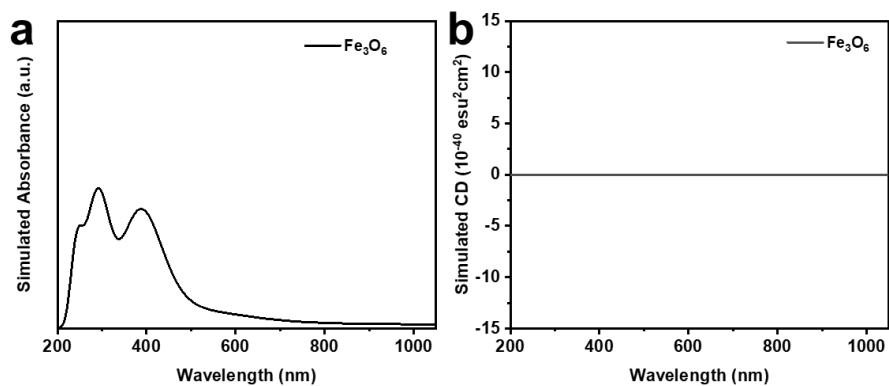


Figure S20. TD-DFT calculation results for Fe_3O_6 . Simulated (a) absorbance, and (b) CD spectra.

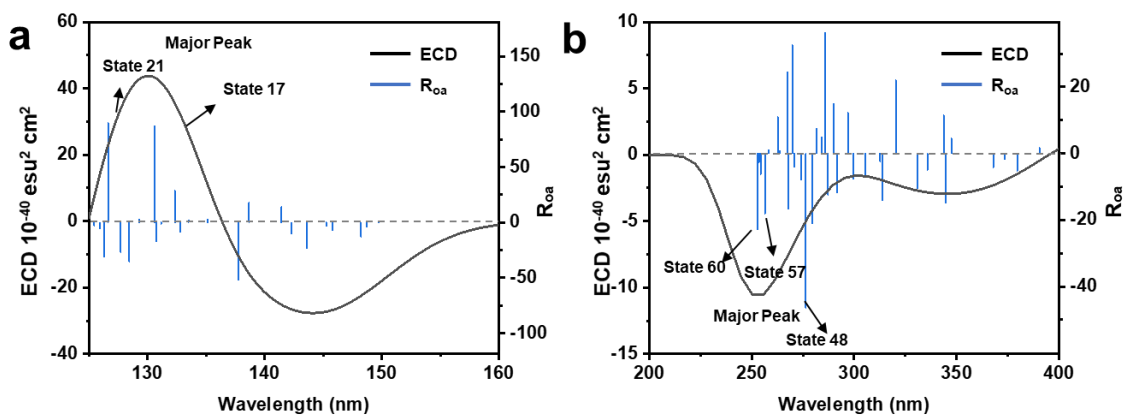


Figure S21. Simulated CD spectra for (a) Glu and (b) $\text{Fe}_3\text{O}_6\text{-3Glu}$. The blue lines represent the major excited states.

Table S2. Major excited states for Glu.

Excited State	Wavelength (nm)	R_{oa}	θ (degree)	Cos θ
14	132.33	28.66	46.75	0.685
16	130.71	-17.25	107.24	-0.296
17	130.59	87.44	31.67	0.851
19	128.44	-35.84	134.11	-0.696
20	127.7	-26.71	135.28	-0.711
21	126.63	89.81	21.24	0.932
22	126.28	-30.93	114.78	-0.419
25	124.6	52.76	36.81	0.801

Table S3. Major excited states for Fe₃O₆-3Glu.

Excited State	Wavelength (nm)	R_{oa}	θ (degree)	Cos θ
31	344.46	-14.88	111.74	-0.370
34	330.80	-10.46	103.4	-0.232
35	320.22	21.99	71.03	0.325
36	313.72	-14.03	108.83	-0.323
40	296.85	12.36	78.44	0.200
41	291.55	-11.79	132.5	-0.676
42	289.89	15.00	65.82	0.410
43	287.21	-12.40	165.9	-0.970
44	285.90	36.29	50.15	0.641
47	279.53	-21.07	112.69	-0.386
48	276.38	-46.35	120.15	-0.502
51	269.79	32.62	70.93	0.327
52	267.84	-16.79	120.45	-0.507
53	267.33	24.43	40.72	0.758
57	256.41	-18.10	113.48	-0.398
60	252.83	-22.93	105.17	-0.262

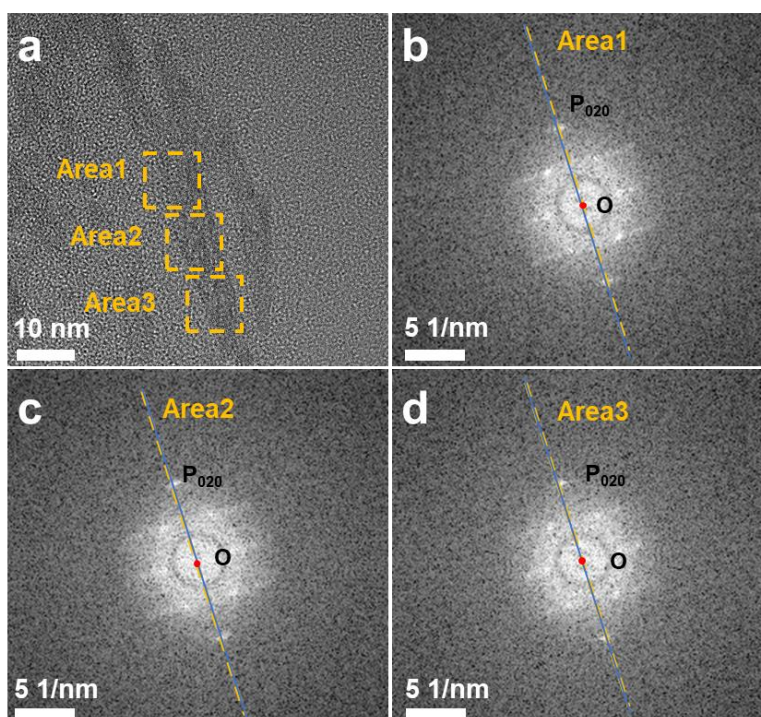


Figure S22. (a) An HRTEM image of CNC-Fe-36. FFT analyses for (b) Area 1, (c) Area 2 and (d) Area 3 shown in a. The blue solid line indicated a fixed direction, and the yellow dashed line connects the origin (O) and P_{020} , which is perpendicular to (020) planes, parallel to the b axis and the growth direction of NWs.

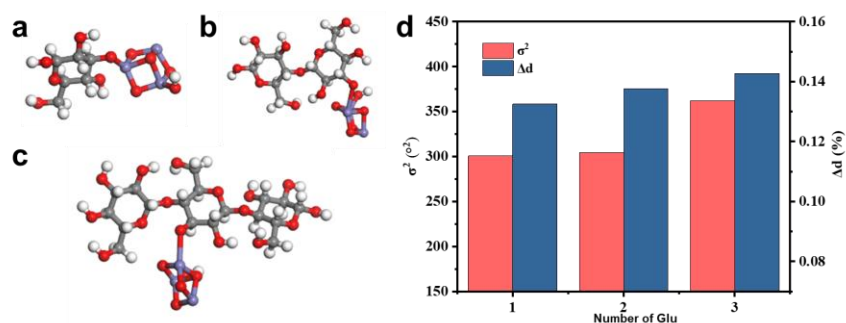


Figure S23. Atomistic models of a) $\text{Fe}_3\text{O}_6\text{-Glu}_1$, b) $\text{Fe}_3\text{O}_6\text{-Glu}_2$, and c) $\text{Fe}_3\text{O}_6\text{-Glu}_3$, where the subscript of Glu represents the number of glucose monomers. d) The influence of the number of glucose monomers on Δd and σ^2 .

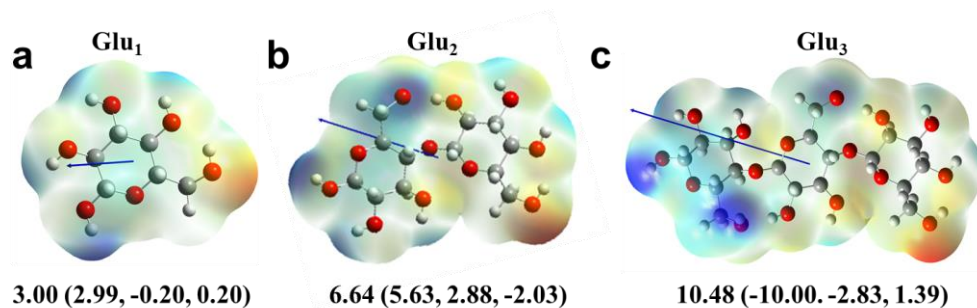


Figure S24. The electrostatic potential distribution and DMs of a) Glu₁, b) Glu₂, and c) Glu₃. Colors toward the blue correspond to positive electrostatic potential. The arrows indicate the direction of DM, which is set to point from negative to positive.

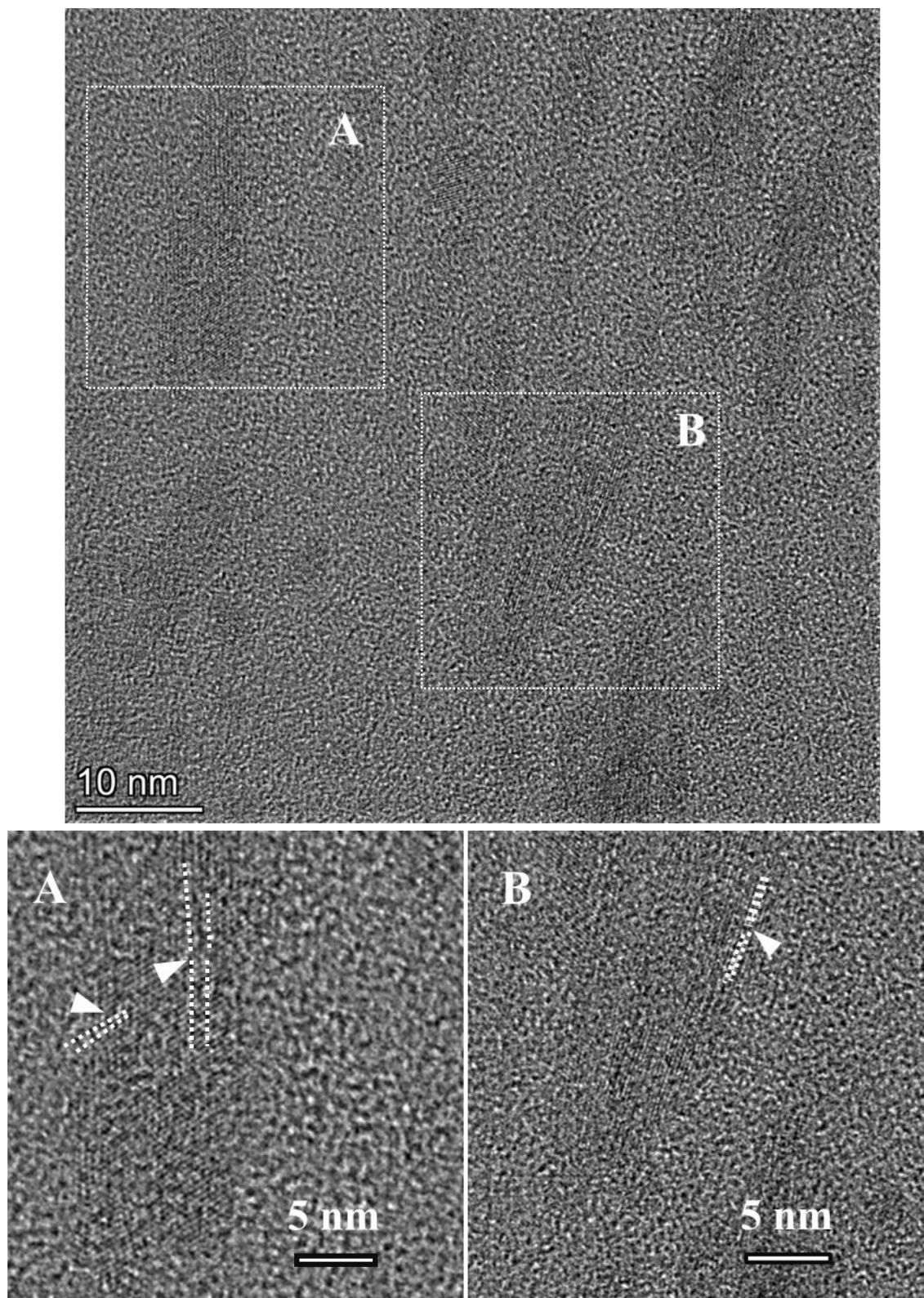


Figure S25. Edge dislocations revealed by HRTEM images of CNC-Fe-36.

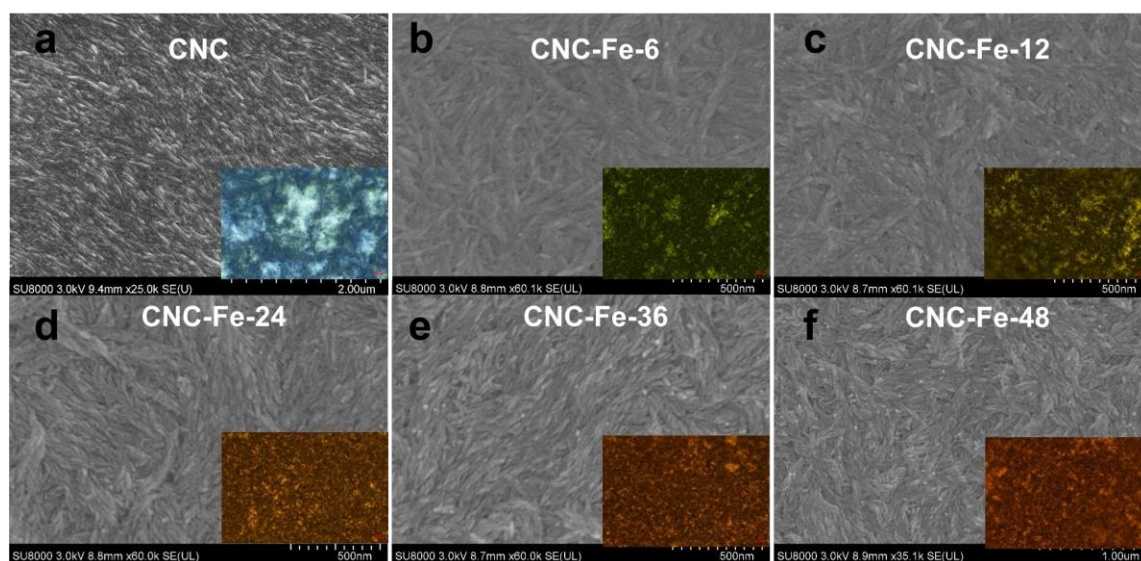


Figure S26. SEM images of the surface of CNC and CNC/ β -FeOOH films. Insets are the corresponding POM images. (a) CNC, (b) CNC-Fe-6, (c) CNC-Fe-12, (d) CNC-Fe-24, (e) CNC-Fe-36, and (f) CNC-Fe-48.

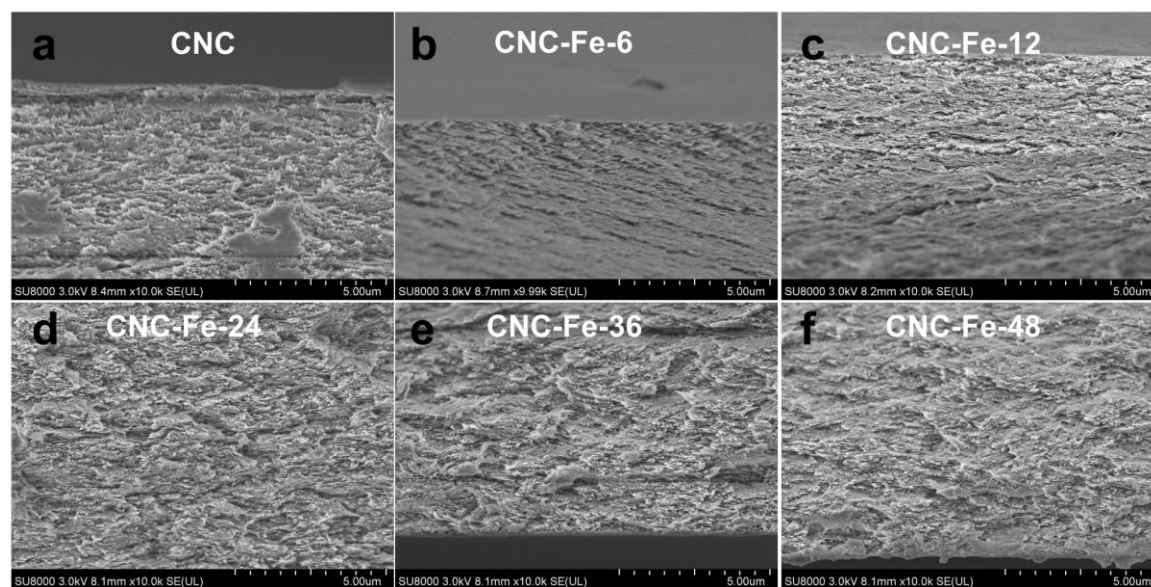


Figure S27. Cross-sectional SEM images of CNC and CNC/ β -FeOOH films. (a) CNC, (b) CNC-Fe-6, (c) CNC-Fe-12, (d) CNC-Fe-24, (e) CNC-Fe-36, and (f) CNC-Fe-48.

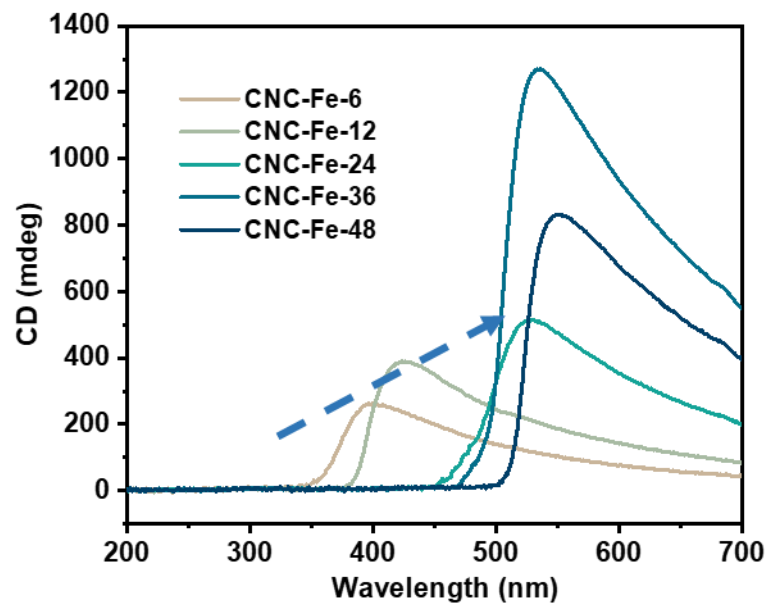


Figure S28. CD spectra of CNC/ β -FeOOH films.

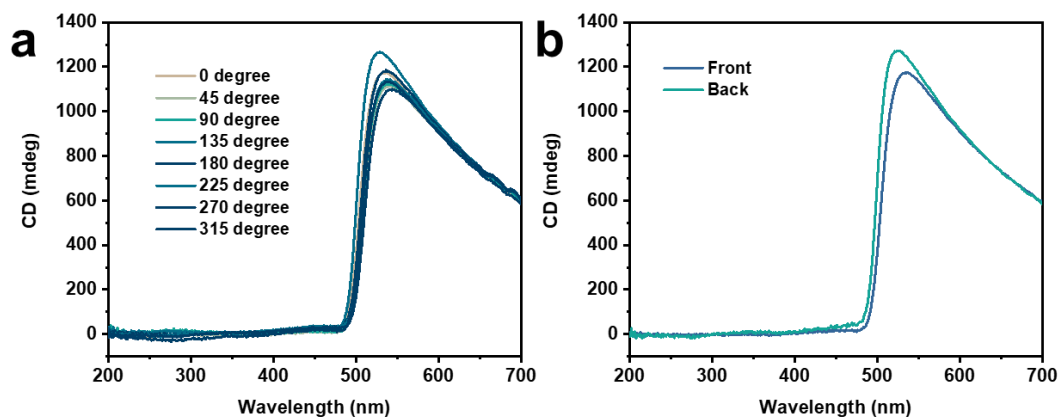


Figure S29. CD spectra of CNC-Fe-36 films after (a) being rotated at different angles normal to the incident light and (b) flip-over.

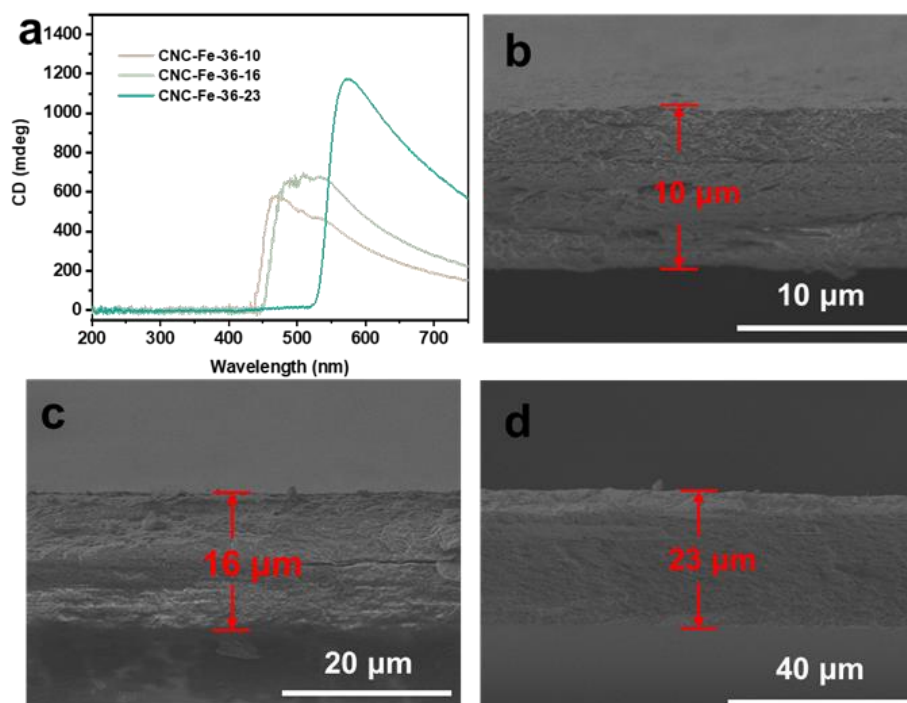


Figure S30. (a) CD spectra of CNC-Fe-36 films with different thicknesses (denoted as CNC-Fe-36-Th, where Th represents the thickness of the film in μm). Cross-sectional SEM images of (b) CNC-Fe-36-10, (c) CNC-Fe-36-16 and (d) CNC-Fe-36-23.

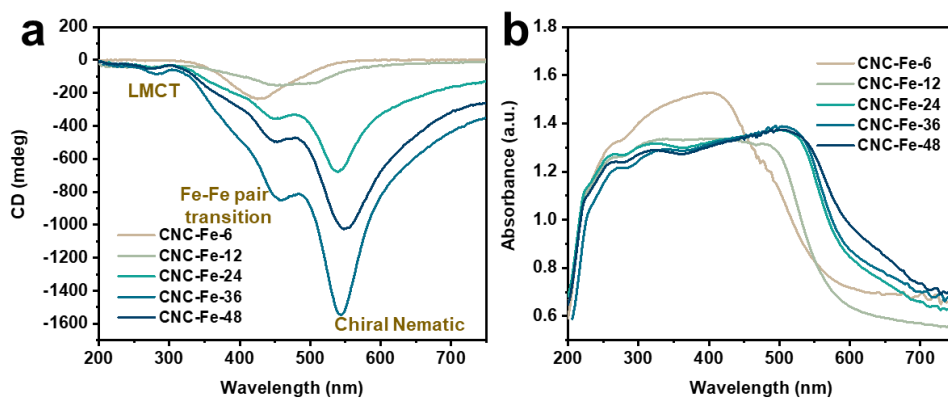


Figure S31. (a) DRCD and (b) UV-vis spectra of CNC/ β -FeOOH films recorded under the reflectance mode.

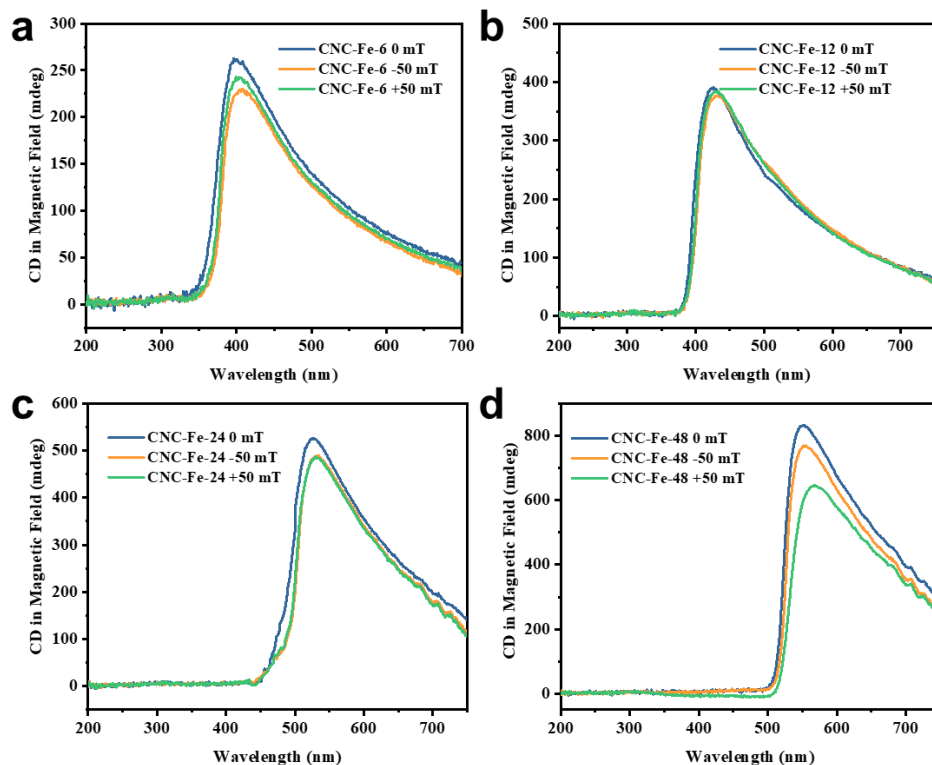


Figure S32. The effect of magnetic field on CD spectra of CNC/ β -FeOOH films. (a) CNC-Fe-6, (b) CNC-Fe-12, (c) CNC-Fe-24, and (d) CNC-Fe-48.

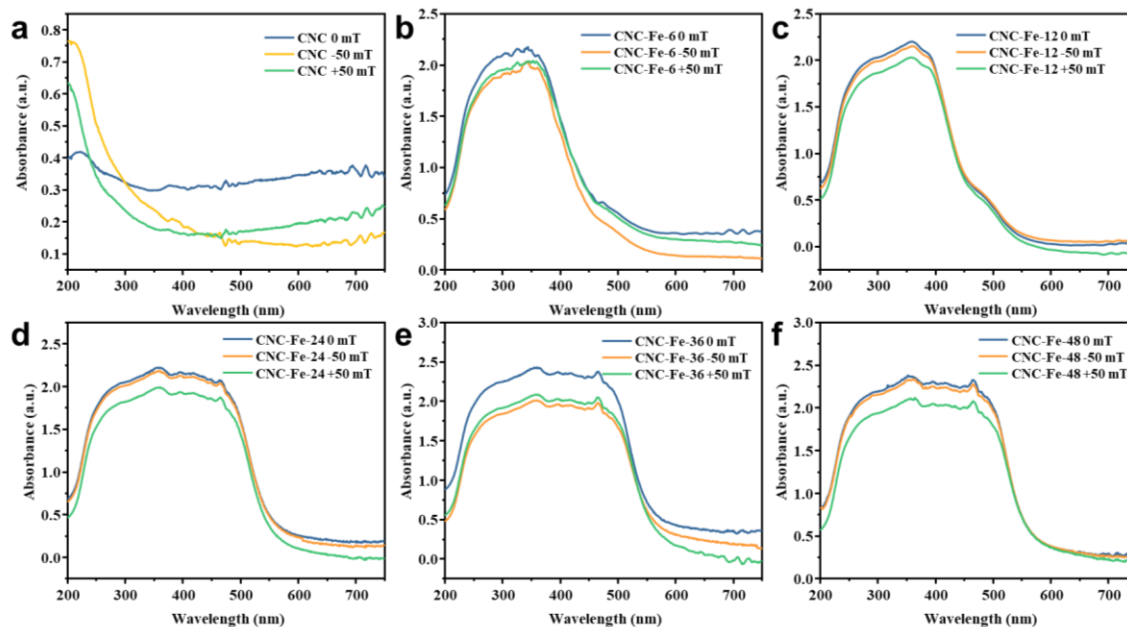


Figure S33. The effect of magnetic field on UV-vis spectra of CNC and CNC/ β -FeOOH films. (a) CNC, (b) CNC-Fe-6, (c) CNC-Fe-12, (d) CNC-Fe-24, (e) CNC-Fe-36, and (f) CNC-Fe-48.

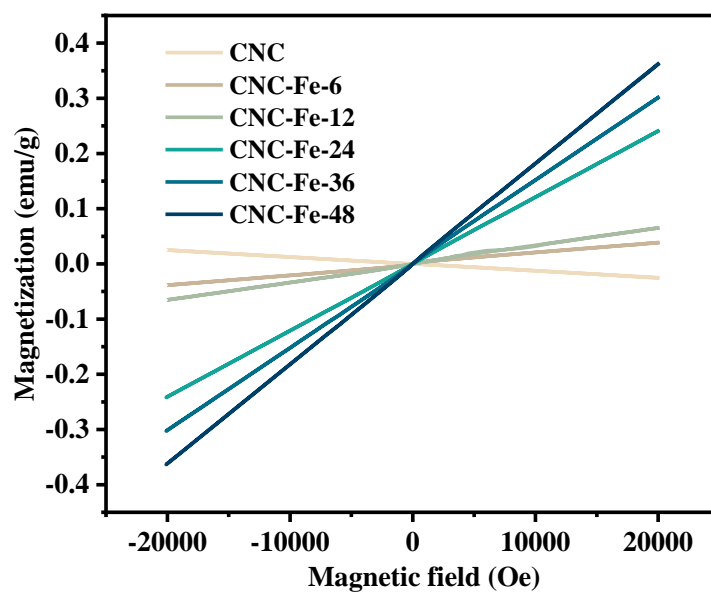


Figure S34. M-H curves of CNC and CNC/ β -FeOOH films at 298 K.

Section S2. The One-Electron Theory Based on the Static Coupling Mechanism

In the framework of the one-electron theory, we consider the influence of local electrostatic fields generated by the permanent charge distribution within a perturbing group. These fields have the potential to distort an original achiral chromophore. As a result, when a light beam interacts with the chromophore, it induces a magnetic dipole aligned in parallel with the electric component of the optical field.

$$\Psi_a = \Psi_a^0 + \sum_{i \neq a} c_{ia} \Psi_i^0$$

$$\Psi_b = \Psi_b^0 + \sum_{j \neq b} c_{jb} \Psi_j^0$$

Where,

$$c_{ia} = \frac{\int \Psi_i^0 V \Psi_a^0 d\tau}{E_a^0 - E_i^0} \quad c_{jb} = \frac{\int \Psi_j^0 V \Psi_b^0 d\tau}{E_b^0 - E_j^0}$$

$$R_{ba} = p_{ab} \cdot m_{ba} + \sum_i c_{ia} (p_{ib} \cdot m_{ba} + p_{ab} \cdot m_{bi}) + \sum_j c_{jb} (p_{aj} \cdot m_{ba} + p_{ab} \cdot m_{ja})$$

$$+ \sum (\text{terms involving products of two } c\text{'s})$$

$$+ \sum (\text{terms involving products of three } c\text{'s}) + \dots$$

Where,

$$p_{ab} = \int \Psi_a^0 p \Psi_b^0 d\tau; p_{ai} = \int \Psi_a^0 p \Psi_i^0 d\tau; m_{ab} = \int \Psi_a^0 m \Psi_b^0 d\tau; \text{ etc.}$$

We will observe that the coefficients, denoted as 'c', are composed of a series of terms representing interactions between individual groups and each chromophore. Consequently,

optical rotation can be understood as the collective result of pairwise interactions between groups, in addition to the summation of products of two such interactions (representing interactions involving three groups at a time), and so forth.

The perturbing field, denoted as V , can typically be considered as the summation of multiple central force fields, V_i . These fields originate from the various groups and atoms surrounding the specific chromophore, with the subscript 'j' referring to the jth atom or group in this context. The computation of any c_{ia} is influenced by V_i , and it entails the calculation of a two-center integral:

$$\int \Psi_i^0 V_j \Psi_a^0 d\tau$$

$$\int \Psi_i^0 V_j \Psi_a^0 d\tau = F(R)f(\theta_x\theta_y\theta_z) + G(R)g(\theta_x\theta_y\theta_z) + \dots$$

$$\int \Psi_i^0 V_j \Psi_a^0 d\tau = F(R)f(\theta_x\theta_y\theta_z)\Phi(\phi_x\phi_y\phi_z) + G(R)g(\theta_x\theta_y\theta_z)\Gamma(\phi_x\phi_y\phi_z)$$

The task of computing optical rotations using the one-electron theory thus involves the calculation of functions that describe the radial and angular dependencies for different field types and states.

$$R_{ba} = \sum_{j,k} \frac{(Ff\Phi + Gg\Gamma + \dots)_{jk}}{E_a^0 - E_k^0} (p_{kb} \cdot m_{ba} + p_{ab} \cdot m_{bk})$$

$$+ \sum_{j,k} \frac{(F'f'\Phi' + G'g'\Gamma' + \dots)_{jl}}{E_b^0 - E_l^0} (P_{al} \cdot m_{ba} + P_{ab} \cdot m_{la})$$

$$g_{ba} = 4 \frac{R_{ba}}{S_{ba}}$$

Rotatory power is anticipated to rely on vicinal interactions. An applied field has the potential to alter the molecular framework, impacting optical rotation's sensitivity to atomic and group positions within the chromophoric groups. If we assume that resistance to distortion follows Hooke's law and the force promoting distortion is field-dependent (reasonable assumptions), a linear relationship between the field and group displacement should emerge, even for significant displacements. Within a small range of displacements, we can reasonably conclude that the effect on optical rotation is proportional to the

displacement amount, thereby establishing a proportional relationship between field and rotivity alteration.